Chapter 10
Femtosecond Filament-Induced Nonlinear Spectroscopy for Combustion Sensing

Huailiang Xu, Helong Li, Hongwei Zang, See Leang Chin and Kaoru Yamanouchi

Abstract Combustion diagnostics is of particular importance in combustion science for raising the combustion efficiency with low-pollution products as well as for monitoring the nanoparticle growth by combustion synthesis. In this chapter, we discuss the feasibility in the detection and diagnosis of combustion intermediates using femtosecond filament-induced nonlinear spectroscopy (FINS) by referring to our recent studies and determine the critical power for self-focusing of a Ti: Sapphire 800-nm, 35-fs laser pulse in alcohol burner flames in ambient air. We find that the laser filamentation in the flame produces a clamped intensity in the range of 2×10^{13}–3×10^{13} W/cm^2 and the flame filament can induce optical emissions from multiple combustion intermediates such as free radicals CH, CN, NH, OH, and C$_2$, as well as atomic C and H. We find that the emission intensities vary sensitively dependent on the fuel species as well as on the positions of the filament within the flame and that the filament can induce nonlinear frequency conversion via harmonic generation, which can be efficiently scattered by soot nanoparticles formed inside the flames. Our results show that FINS has a high potential applicability in remote and in situ sensing of spatial distributions of combustion intermediates in flames.

H. Xu (✉)
State Key Laboratory of Precision Spectroscopy, East China Normal University,
Shanghai 200062, China
e-mail: huailiang@jlu.edu.cn

H. Xu · H. Li · H. Zang
State Key Laboratory of Integrated Optoelectronics, College of Electronic Science
and Engineering, Jilin University, Changchun 130012, China

S. L. Chin
Center for Optics, Photonics and Laser (COPL) and Department of Physics,
Engineering Physics and Optics, Laval University, Quebec City G1V 0A6, Canada

K. Yamanouchi
Department of Chemistry, School of Science, The University of Tokyo, 7-3-1 Hongo,
Bunkyo-ku, Tokyo 113-0033, Japan

10.1 Introduction

Combustion processes through which we release chemical energy stored in the burning fuels generate heat and power that could greatly benefit people to live on our planet. On the other hand, the combustion can also result in a huge number of pollutants such as soot, SO_x, and NO_x, giving rise to serious environmental problems. Therefore, combustion diagnostics that can help understand combustion processes and enhance combustion efficiencies with low-pollution products is of special importance in combustion science. So far, a variety of measurement techniques have been developed for probing the combustion intermediates and products in various combustion environments [1–5]. Among these methods, laser spectroscopic techniques, such as planar laser induced fluorescence (PLIF), infrared spectroscopy and polarization spectroscopy have been extensively employed for measuring combustion temperature, sensing combustion intermediates, and mapping fuel distributions because of their non-invasive, real-time and high-sensitivity characteristics. For example, the PLIF technique can be applied to obtain directly the two-dimensional distribution of the combustion intermediates of OH, CN, CH and CH_2O in a combustion flame with high detection sensitivity [6]. Nevertheless, there are also some technical limitations on these methods. For instance, because PLIF is a resonant technique, it requires a specific laser wavelength to be in resonance with the species to be probed. Since the excitation wavelengths of different species vary in a wide spectral range, which could not be achieved with only one laser source, PLIF can be applied in most cases for the detection of one species at a time. It is true that Raman spectroscopy is a powerful technique for simultaneous sensing of multiple molecular species, but the strong background emissions from the flame itself could mask the Raman signal, leading to a low signal-to-noise ratio. Laser-induced breakdown spectroscopy (LIBS) is another powerful multiple elemental analysis technique, but LIBS involves detecting various atomic species, which makes it difficult to provide the information on the combustion intermediates that are in most cases molecular species.

Recent progress in high-power femtosecond laser technology can produce laser pulses in a wide power range from a sub-terawatt (TW) up to Petawatt (PW). When such powerful laser pulses propagate in transparent optical medium, filamentation takes place as a result of the dynamic balance between Kerr self-focusing and defocusing induced by plasma generated by multiphoton and/or tunnel ionization of the optical medium, giving rise to a long weak plasma channel [7–9]. In air, the dynamic balance limits the laser intensity to an almost constant value of 10^{13}–10^{14} W/cm^2. This is called clamped intensity in the filament core [9]. The filament could be very long ranging from centimeters to near kilometer and could be formed at a far distance [9]. Filamentation in air can initiate a variety of intriguing phenomena such as remote air lasing, THz radiation and high-harmonic generation [10–15]. In particular, as conceptualized in Fig. 10.1, characteristic optical emissions generated from the ionized or fragmented particles in filaments can be investigated by filament-induced nonlinear spectroscopy (FINS), which was proposed as an efficient technique applicable for remote sensing of trace chemical and biological agents and pollutants in

Fig. 10.1 Concept of combustion diagnostic based on femtosecond laser filament-induced nonlinear spectroscopy. The self-channeling laser-induced intense laser intensity induces the ionization and excitation of combustion intermediates which emit characteristic optical radiations. Inset shows a photo of a laser-induced filament in a combustion flame in air with a methanol fuel gas produced by the irradiation of near-IR femtosecond laser pulses (800 nm, 40 fs, and 5.5 mJ/pulse)

the atmosphere [16–20]. This technique is applicable even in a harsh atmospheric environment [9]. Based on the detection characteristics of FINS mentioned above, we recently reported that the FINS technique can have a high potential for a diagnosis of multiple intermediate species generated in complex combustion environments [20].

In this chapter we shall discuss the feasibility of the FINS technique in detection and diagnosis of combustion intermediates by referring to our recent studies of femtosecond laser filamentation in combustion flames. We will first show in Sect. 2 the formation of filamentation in combustion (flames) and the determination of the two fundamental physical properties; i.e. the critical power for self-focusing and the clamped intensity. In Sect. 3, we will present the typical fingerprint spectra induced by laser filamentation in flames and discuss the feasibility of the FINS technique for the detection of combustion intermediates in flames fueled by different alkanol molecules. In Sect. 4, we will show third harmonic generation and scattering in flames using femtosecond laser filaments for sensing soot nanoparticles. Finally, in Sect. 5, a summary will be given.

10.2   Filamentation in Combustion Flames

For the formation threshold and properties of femtosecond laser filamentation in combustion flames, we performed experiments to measure the two fundamental physical parameters: (i) the critical power for self-focusing of Ti: Sapphire 800 nm laser pulses, and (ii) the laser intensity clamped in the filament core [21]. The former determines whether filamentation could be formed, and the latter is crucial for understanding the nonlinear filament-flame interaction. Both of them are sensitive to the propagation media.

10.2.1   Critical Power

It is well known that, when the peak power of the laser pulse is smaller than the critical power, the focal position of the laser beam keeps practically constant at the geometrical focus due to the absence of the Kerr self-focusing effect [9]. However, when it exceeds the critical power, the pulse will collapse towards a self-focus due to the self-focusing that makes the medium equivalent to an additional focal lens [22]. Combined with the external focal lens, it leads to a shift of the focal position from the geometrical focus toward the position of the focusing lens [9, 22, 23]. Therefore, by measuring the focal position as a function of the input laser energy, the critical power can be straightly determined as the power at which the focal position starts to move.

   In the measurement, a Ti: Sapphire laser system (Spectra Physics, Spitfire) was used, which produced laser pulses with a central wavelength at 800 nm, a pulse duration of 35 fs and a repetition rate of 1 kHz. A half-wave plate and a Brewster window were inserted into the laser beam for adjustment of the pulse energy. The laser pulses were focused by an $f = 50$ cm fused silica lens into an ethanol-air flame on an alcohol burner array. The flame has a length of about 5 cm, and a height of about 40 mm. The distance between the laser focal position and the burner wick was about 9 mm. The 'fluorescing' filament was imaged onto the entrance slit of a spectrometer coupled with a gated intensified charge coupled device (ICCD, Andor iStar) by using a periscope and a fused silica lens (50.8 mm in diameter, $f = 6$ cm). The fluorescence was then dispersed by a grating with 1200 grooves/mm whose blazed wavelength is 500 nm and recorded by the gated ICCD camera. The ICCD gate was opened for 10 ns prior to the arrival time of the laser pulse at the interaction zone and the gate width was set to be $\Delta t = 210$ ns.

   When we focused a 500 μJ femtosecond laser pulse on the ethanol-air flame in the ambient atmosphere, the spectrum in Fig. 10.2a was obtained. The emission signals were assigned to the electronic transitions of free radicals CH, CN, N_2, NH, OH, and C_2. When the pump laser energy was decreased to be lower than the critical power, the intensities of the laser-induced emissions from the combustion free radicals of CH, OH, and C_2 were found to become comparable to or even weaker than their
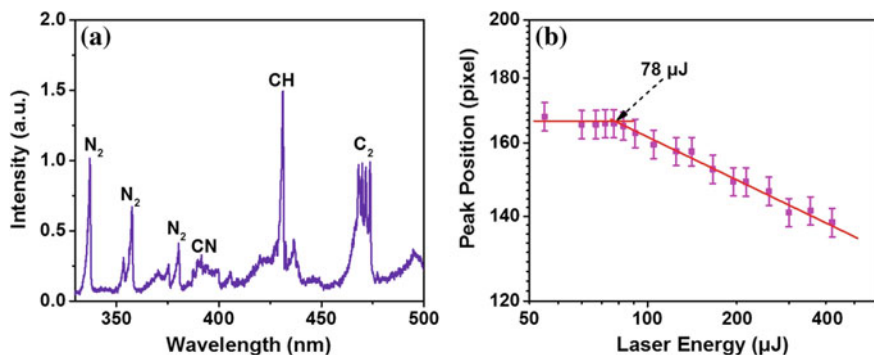
Fig. 10.2 (a) Optical emission spectrum induced by ultrafast filamenting laser pulses in an ethanol-air flame. (b) The focal position determined using the nitrogen fluorescence signals in the flames as a function of the input laser energy

spontaneous emissions in the flame, as explained below in Sect. 10.3. In addition, the fluorescence emission intensities from CN and NH, which are generated mainly through the chemical reactions proceeding in the laser-induced plasma, were found to become too weak when the laser intensity was lowered. Therefore, the fluorescence emission of N_2 at 337 nm was used for monitoring the shift of the self-focal position in response to the variation of the input laser intensity.

In Fig. 10.2b, the focal position determined from the measurements of the spatial distribution of the N_2 fluorescence signals at 337 nm along the laser propagation is plotted as a function of the input laser energy. It can be seen that when the laser power is weaker than a certain value, the focal position keeps at an almost constant position, showing the absence of self-focusing effect. However, when the laser power increases, the focal position moves towards the focusing lens. By fitting the data shown in Fig. 10.2b using two straight lines, the critical energy for the self-focusing of the employed laser pulses in the ethanol-air flame was determined to be ~78 μJ. Therefore, the critical power was calculated be ~2.2 GW, which is about four times smaller than that in air (10 GW for near IR (800 nm) 42 fs laser pulses [23]).

According to the measured critical power and the theoretical relation of $P_c = 3.72\lambda^2/8\pi n_0 n_2$, where n_0 and n_2 are the linear refraction index and the second order nonlinear index coefficients of a pure gas, respectively, we can calculate the numerical value for the effective second order nonlinear index coefficient in the flame. Because the flame was produced in ambient air, we assumed the linear index of refraction to be $n_0 = 1$, and obtained an effective value of $n_2 = 40 \times 10^{-20}$ cm^2/W, which is about four times as large as that of air (12×10^{-20} cm^2/W) [24].

10.2.2   Clamped Intensity

In the determination of the clamped intensity of the filament inside the flame, we adopted a simple method by which the intensity can be calculated from the laser pulse energy transmitted through a pinhole drilled on a metallic foil by the filament and the pinhole area. In this measurement, the laser beam was loosely focused into the ethanol-air flame by a 1-m fused silica lens. The repetition rate of the laser pulses was changed to 100 Hz and the laser energy was fixed at 0.8 mJ. The corresponding peak power was higher than the critical power for the self-focusing. A mechanical shutter was placed just before the focal lens to control the number of laser pulses. A 50 μm-thick copper foil was inserted into the flame with the surface perpendicular to the laser propagation direction. A power meter was used to record the laser energy transmitted through the pinhole drilled by the filament itself on the copper foil. The area of the drilled pinhole was measured by a scanning electron microscope (JEOL JSM-7500F). As a reference, a similar experiment in air was also performed.

In Fig. 10.3, we show the transmitted laser pulse energy as a function of the number of the laser shots, from which we find that the transmitted laser energy increases as the number of laser shots increases. In addition, it can be noted from the linear fits of the data shown in Fig. 10.3 that the transmitted laser pulse energy first increases linearly with a larger slope, and then, after 700 laser shots, the slope becomes shallower. The observation of the two linear regions can be explained as follows. The steeper slope before 700 laser shots shows that the laser energy inside the filament core passes the pinhole as shown by the SEM image in the inset of Fig. 10.3 while the energy in the reservoir surrounding the filament core is blocked by the pinhole, so that the drilled pinhole area can represent the cross section of the filament core. The shallower slope after 700 laser shots reflects the fact that the wandering effect of the filament becomes dominant, which enlarges the area of the drilled pinhole [25]. Therefore, the clamped intensity can be determined from the measured laser energy and the pinhole area at the crossing position of the two slopes at 650 laser shots, which is about $I_{f(\text{obs})} \sim 5.2 \times 10^{13}$ W/cm^2. As a reference, we also performed the same measurement in air by removing the flame from the optical path, which gave a clamped intensity of $I_{a(\text{obs})} \sim 1.2 \times 10^{14}$ W/cm^2. This measured value of I_a is 2.4 times as large as the commonly quoted value of $I_a^{(0)} = 5 \times 10^{13}$ W/cm^2 in air [9], which indicates that we overestimated the clamped laser intensity in the flame by a factor of 2.4. Therefore, we obtain $I_{f(\text{obs})}^{(0)} = 2.2 \times 10^{13}$ W/cm^2 as the calibrated clamped intensity inside the frame by dividing $I_{f(\text{obs})} \sim 5.2 \times 10^{13}$ W/cm^2 by 2.4. As a next step, in order to correct the beam wandering effect, which makes the slope shallower when the number of the laser shots becomes larger than 700, the correction factor $r = 1.3$, defined as the ratio of the steeper slope with respect to the shallower slope, was obtained, and the corrected clamped laser intensity in the flame was derived as $I_{f(\text{obs})}^{(\text{cor})} = r \times I_{f(obs)}^{(0)} = 2.8 \times 10^{13}$ W/cm^2. This means that, as has been pointed out in [21], the clamped laser field intensity in combustion flames is about a half of the clamped laser field intensity in air, $I_a^{(0)} = 5 \times 10^{13}$ W/cm^2 [9].

Fig. 10.3 The measured transmitted laser energy as a function of the number of laser shot. Inset: the SEM image of the pinhole drilled on a copper foil by the filament itself with 650 laser shots
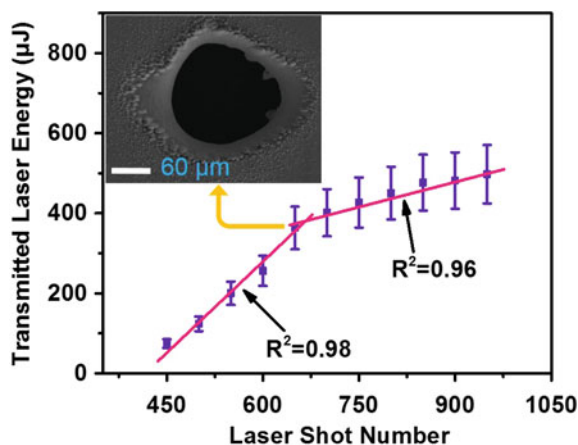
## 10.3 FINS in Combustion Flames

Although the clamped intensity in combustion flames is only a half of that in air, the intensity is high enough to induce nonlinear optical interactions with the combustion species, resulting in characteristic fluorescence emissions. In this section, we investigate the filament-induced fluorescence spectra in combustion flames, and discuss the feasibility of FINS for combustion diagnosis.

10.3.1 Filament-Induced Fluorescence

Figure 10.4 shows a typical filament-induced spectrum of the ethanol-air flame in ambient atmosphere in the spectral range from 240 to 850 nm [26]. This spectrum was obtained by focusing the laser pulses (800 nm, 100 fs, 0.7 mJ) into the alcohol burner flame by a fused silica lens ($f = 200$ mm), which generated a filament of 1 cm. The width and delay of the ICCD gate were set to be $\Delta t = 2000$ ns and $t = 0$ ns, respectively. The distance between the filament and the tip of the burner wick was 18 mm. The total length of the flame from the burner wick to the top of the flame is ~50 mm. The spectral signals are assigned to the Swan band of C_2 radical (563, 516, and 466 nm), CH radical resulting from the $A^2\Delta$-$X^2\Pi$ (431 nm) and $C^2\Sigma$-$X^2\Pi$ (314 nm) band, and CN radical originating from the $B^2\Sigma$-$X^2\Sigma$ (388 and 358 nm) band, respectively [27]. In addition, several weak emission bands assigned to molecular species such as N_2 (337 nm), NH (336 nm) and OH (307 nm) and atomic emission lines assigned to atomic species, C (247.7 nm) and H (Balmer-α, 656 nm), can be seen.

For removing the second order diffraction and the third order diffraction of the fluorescence emission in the UV wavelength range from the spectrum as well as for

Fig. 10.4 Typical FINS spectrum obtained by focusing a 0.7 mJ femtosecond laser pulse into an ethanol-air flame in ambient air
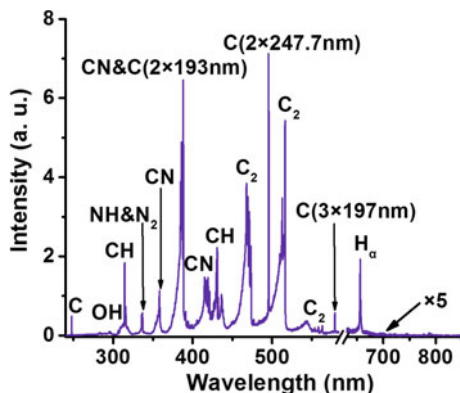
extracting the spectral information in the long wavelength range with high precision, a high-pass filter was placed before the spectrometer slit to block the signal below 450 nm. As shown in Fig. 10.4, except for H_α (Balmer-α) line at 656 nm, no atomic emission lines such as N (I) at 744 nm and O (I) at 777 and 845 nm are observed, which are typically present in nanosecond laser-induced breakdown spectroscopy, in which optical emission lines from electronically excited fragment species generated from parent molecules. Therefore, we concluded that the fragmentation and electronic excitation processes proceeding in the laser induced filament in the flame are much milder than those in the nanosecond laser induced breakdown. Therefore, FINS is considered to be a promising technique for monitoring the combustion intermediates in flames.

10.3.2 Mechanisms for the Fluorescence Emissions from Radicals in FINS

As described in Sect. 2, the laser intensity in the filament in a combustion flame is clamped to be ~2.8 × 10^13 W/cm^2. For a so high intensity, it was questioned whether the filament-induced fluorescence results from the dissociation and fragmentation of parent molecules. Therefore, we performed a comparative study by measuring the flame spectra under different conditions, that is, with the excitation of femtosecond filament, nanosecond laser-induced breakdown as well as without laser excitation [26].

Figure 10.5a shows a typical ns-LIBS spectrum of the ethanol–air flame, which we obtained by focusing 532-nm Nd: YAG laser pulses into the ethanol-air flame using a fused silica lens of 125 mm. The laser pulse duration and energy were 10 ns and 100 mJ, respectively. The width and delay of the ICCD gate were set to be the same as those in the FINS measurement presented in Sect. 3.1. By comparing the LIBS spectrum with that shown in Fig. 10.4, it can be seen that LIBS shows atomic/ionic
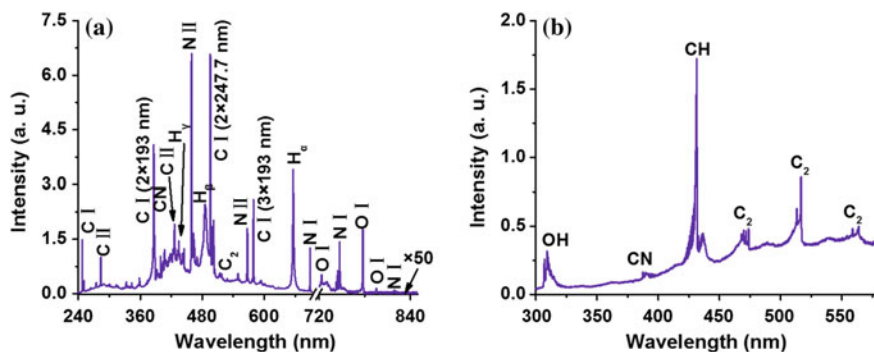
Fig. 10.5 a Typical LIBS spectrum obtained when a 100 mJ, 10 ns laser pulses were focused into an ethanol-air flame in ambient air using an $f = 125$ mm lens. **b** Emission spectrum of the flame recorded without any laser excitation

lines, which are superposed on a broad continuum. These intense atomic emission lines can be assigned to the Balmer lines (H_α, H_β, and H_γ), and the emission lines of C(I, II), N (I, II) and O (I). The FINS (Fig. 10.4) spectrum, in which emission lines of molecular species dominate, confirms that the decomposition and electronic excitation do not proceed in an excessive manner in the femtosecond filamentation in the flame, exhibiting a marked contrast with the LIBS (Fig. 10.5a) spectrum, in which emission lines from the electronic excited states of fragment atoms and atomic ions dominate.

The emission spectrum of the ethanol–air flame without laser excitation was also measured as shown in Fig. 10.5b, in which the molecular emission bands of the intermediate molecular species such as OH, CH and C_2 created in the combustion flame can be observed together with a broad continuum originating from the blackbody radiation of the flames. The accumulation time was set to be 450 ms.

As can be seen in the FINS spectrum (Fig. 10.4) and the laser-free flame spectrum (Fig. 10.5b), all of the free radical species appearing in the laser-free flame spectrum appear also in the FINS spectrum, indicating that FINS carries the information on the intermediates of the combustion flame. However, it should be noted that the ratios of the relative signal intensities of combustion species OH, CH, CN and C_2 are obviously different in these two cases. For example, the signal of CN at 388 nm is much stronger in FINS than that in the laser-free flame spectrum, which implies that a part of the CN emission lines appearing in FINS originate from bimolecular chemical reactions, such as $C_2 + N_2$, though which CN is prepared in the electronically excited states in the filament-induced plasma.

It can also be seen that the ratio of the signal intensity of CH at 431 nm with respect to that of C_2 at 516 nm is much smaller in FINS than that in the laser-free frame spectrum. It is well known that the dissociation of the parent ethanol molecule in intense laser fields prefers to form CH than C_2 [28], the smaller ratio of CH/C_2 in FINS may indicate that the CH radical are not produced from the dissociation of the

parent fuel molecule, and that the plasma-assisted collision might give a contribution to the formation of C_2 in FINS.

We also performed the FINS measurements at the different spatial positions in the flames, by moving the burner vertically and found that the intensities of all the free radical species in FINS become weaker when the position becomes closer to the wick of the alcohol burner [29]. Because the concentration of the parent fuel molecules is higher at the positions closer to the burner wick, the observation clearly indicates that the dissociation of the parent fuel molecules induced by the intense laser fields in the femtosecond filament may not contribute to the FINS signals. Therefore, it can be said that the combustion intermediates appearing in FINS are not those created by the fragmentation of parent fuel molecules but those excited electronically by the femtosecond laser light and/or collisions within the laser induced filament in the combustion flame.

10.3.3   Feasibility of FINS for Combustion Diagnostics

In order to further explore the possibility of the application of FINS to the sensing of combustion intermediates, we systematically investigated the FINS phenomena in various environmental conditions. We first measured the FINS spectra at the different spatial positions in the ethanol-air flame along the vertical axis of the central combusting flow, and plotted the signal intensities of different combustion intermediates as a function of the distance between the filament and the wick tip of the alcohol burner [29]. As shown in Fig. 10.6a, the signals of the four species, C_2, CH, CN and C, first increase and then decrease as the distance increases, which reflects the concentration distribution of the four intermediate species in the flame. In the region just above the burner wick the combustion has not been fully developed, resulting in a low concentration of combustion intermediates. As the distance increases, the combustion further develops, resulting in the formation of a large number of combustion intermediates, and thus the increased fluorescence signals. When the distance increases further, the combustion intermediates are consumed in the fully developed combustion zone, resulting in the decreased signals. This result shows the possibility to map the concentration distributions of combustion intermediates using the FINS technique.

We also performed the FINS measurements for five different alkanol-air flames fueled by methanol, ethanol, *n*-propanol, *n*-butanol, and *n*-pentanol [30]. The analysis of the FINS spectra of the five different alkanol-air flames showed that the combustion reactions with the five different fuels produce almost the same combustion intermediate species. This means that the combustion intermediate species can be the same as long as fuel molecules are composed of the same elements, that is, C, H and O. On the other hand, the spectral intensities of the four main combustion intermediates C, C_2, CH, CN increase as the number of carbons contained in a single fuel molecule increases. It was also found that the ratios of the signals of these intermediates produced in the five different alkanol combustion flames exhibit char-
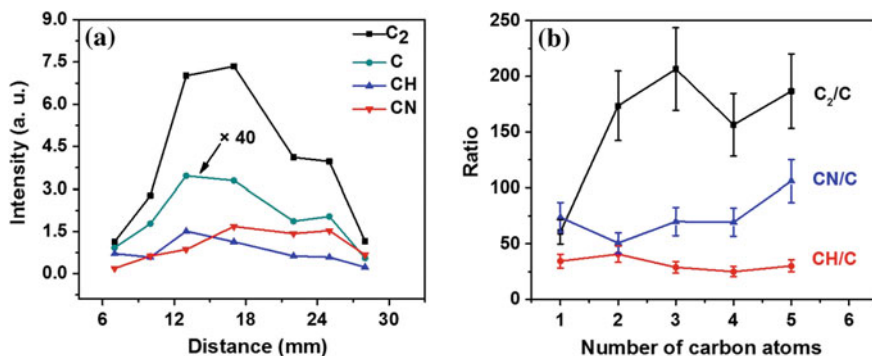
Fig. 10.6 a Signal intensities of the four filament-induced combustion intermediates, C_2, C, CH, and CN, in the ethanol flame recorded by the FINS measurements as a function of the distance between the filament and the tip of the alcohol burner wick. **b** The ratios of the signal intensities of the three combustion intermediates with respect to the signal intensity of C for the five different fuel molecules, methanol ($m = 1$), ethanol ($m = 2$), n-propanol ($m = 3$), n-butanol ($m = 4$), and n-pentanol ($m = 5$), where m stands for the number of carbon atoms within a fuel molecule

acteristic dependences on the number of carbon atoms in a fuel molecule as shown in Fig. 10.6b. Therefore, by the FINS measurements, alkanol species that are fueled for producing the alkanol-air flames can be readily identified based on the intensity ratios of the combustion intermediates.

10.4 Third Harmonic Generation in Flames

Femtosecond filamentation generated by 800-nm Ti:Sapphire laser pulses induces not only nonlinear fluorescence emission but also nonlinear frequency conversion. In this section, we investigate third harmonic generation inside the combustion flames using femtosecond laser filaments and show a potential applicability of Rayleigh scattering spectroscopy using the third-harmonics in the UV range to remote and in situ measurements of distributions of soot nanoparticles in combustion flames [31].

10.4.1 Third Harmonic Generation in Flames

Figure 10.7a shows the forward third harmonic spectra induced by the filamentation in air as well as in the alkanol–air flames fueled with methanol, ethanol, n-propanol, n-butanol, and n-pentanol. In this measurement, the laser pulses whose pulse energy is 0.6 mJ was focused by a fused silica lens ($f = 50$ cm) into the flame and a single filament was generated. The filament position was set to be at about 28 mm above the
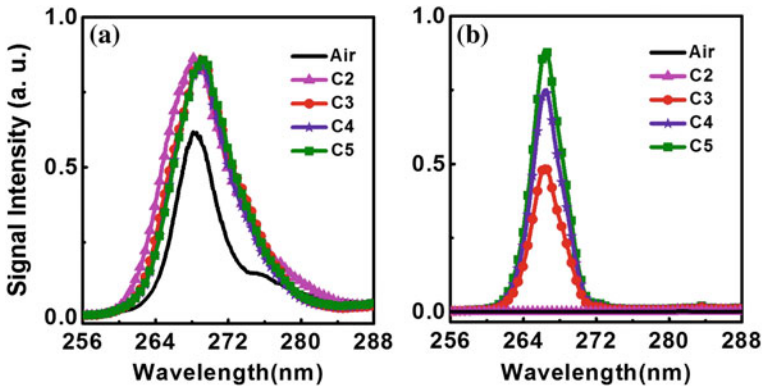
Fig. 10.7 Third harmonic signals measured from the forward direction along the laser propagation (**a**) and those measured from the side of the filament (**b**) for air and the four different flames fueled with ethanol, *n*-propanol, *n*-butanol, and *n*-pentanol

tip of the alcohol burner wick. The third harmonic produced by the femtosecond laser filamentation in the flame was measured in the forward direction after the attenuation using two wedge plates. The width and delay time of the ICCD gate were set to be $\Delta t = 20$ ns and $t = -5$ ns, respectively. As shown in Fig. 10.7, the third harmonic at ~267 nm was generated by the laser induced filament in air as well as in the four different flames.

It can be seen in Fig. 10.7a that the signal intensities of the filament-induced third harmonic in the combustion flames are almost the same for all the four alkanol species, showing that the third harmonic generation is not sensitive to the fuel species used in our experiment. It can also be seen that the third harmonic generated in the flames are stronger than that in air, which may be explained as follows. The intensity of the generated third harmonic is expressed using the clamped laser intensity in the filament I_{clamp} as $I_{harmonic} \propto (n_0 n_2)^2 (I_{clamp})^3$. As determined in Sect. 2.1, the value of n_2 in the ethanol-air flame (40×10^{-20} cm^2/W) was about four times larger than that in air (12×10^{-20} cm^2/W), and the clamped laser intensity in the flame filament was about 56% of that in air. Therefore, the intensity of the filament-induced third harmonic in the ethanol-air flames is expected to be roughly twice as large as that in air, which is in good agreement with the experimental observation shown in Fig. 10.7a. The observation shown in Fig. 10.7a that the third harmonic intensities for all the four alkanol-air flames are almost the same indicate that the second order nonlinear refractive index coefficient n_2 and the clamped laser intensity I_{clamp} for these four fuel species are close to each other.

We also examine the dependence of the conversion efficiency in the third harmonic generation in the flame filaments on the polarization state of the fundamental laser light. By rotating a quarter wave plate inserted in the fundamental laser beam with which the polarization of the fundamental laser light can be varied from linear to

circular, we find that the intensity of the third harmonic signals decreases dramatically as the polarization of the fundamental laser changes from linear to circular [31].

10.4.2   Third Harmonic Scattering in Flames

In order to examine the scattering of the third harmonic by the soot particles produced in the combustion flames, we measured the third harmonic from the side of the laser filament. Because the third harmonic propagates along the propagation direction of the fundamental laser pulse, the signal intensity of the third harmonic recorded from the side of the filament can be regarded as the scattering of the particles in the combustion flame. The experimental conditions were the same as in the measurement from the forward direction. For collecting the emission signal, we employed a $2f$–$2f$ imaging scheme with a fused silica lens of $f = 60$ mm.

As shown in Fig. 10.7b, the intensity of the scattered third harmonic signals from the four alkanol-air flames increases as the number of carbon atoms in the fuel molecular species increases whereas no signals of the scattered third harmonic can be seen in air. This is because the third harmonic signals are scattered by carbonous nanoparticles existing in the flames originating from the incomplete combustion, which are typically from a few to tens of nanometers [3, 32], and because the number density of the nanoparticles in the flames increases as the carbon number in the fuel molecule increases. Therefore, the filament-induced third harmonic spectroscopy can be used for monitoring the density distribution of nanoparticles in combustion flames. The observation that no detectable scattering signals of the third harmonic were recorded in air indicates that the number density of carbonous nanoparticles was considerably low in air in the laboratory environment.

10.5   Summary

In this chapter, by referring to our recent studies on femtosecond laser filamentation in combustion flames, we show the feasibility of the detection and diagnosis of combustion intermediates using femtosecond filament-induced nonlinear spectroscopy (FINS). By measuring the focal positions of ultrafast laser pulses versus the laser energy, and comparing the difference of the laser energy transmitted through a pinhole drilled on a metallic foil by the filament itself, we determined the critical power and the clamped intensity of femtosecond laser filaments in combustion flames in ambient air. We further demonstrated that the clamped intensity in combustion flames is high enough to induce characteristic optical emissions from multiple combustion intermediates, and found that the intensities of these intermediate emissions vary sensitively to the fuel species as well as the positions of the filament within the flame. We also introduced the phenomena of the filament-induced third harmonic generation in flames and demonstrated that the third harmonic can be efficiently scattered

by nanoparticles formed in flames. We demonstrated that FINS has a high potential applicability to remote and in situ sensing of the spatial distributions of combustion intermediates in flames as well as to combustion diagnostics for understanding the combustion processes, leading to a new scheme with which the combustion efficiency is to be raised with low-pollution products.

References

1. N. Docquier, S. Candel, Prog. Energy Combust. Sci. **28**, 107 (2002)
2. G. Hagen, C. Feistkorn, S. Wiegärtner, A. Heinrich, D. Brüggemann, R. Moos, Sensors **10**, 1589 (2010)
3. M. Aldén, J. Bood, Z. Li, M. Richter, Proc. Combust. Inst. **33**, 69 (2011)
4. A.C. Eckbreth, *Laser Diagnostics for Combustion Temperature and Species*, 2nd edn. (Gordon & Breach, UK, 1996)
5. S. Svanberg, *Atomic and Molecular Spectroscopy: Basic Principles and Practical Applications* (Springer, Berlin, 2004)
6. J. Sjöholm, J. Rosell, B. Li, M. Richter, Z. Li, X.S. Bai, M. Aldén, Proc. Combust. Inst. **34**, 1475 (2013)
7. A. Couairon, A. Mysyrowicz, Phys. Rep. **441**, 47 (2007)
8. L. Berge, S. Skupin, R. Nuter, J. Kasparian, J.-P. Wolf, Rep. Prog. Phys. **70**, 1633–1713 (2007)
9. S.L. Chin, *Femtosecond Laser Filamentation* (Springer, Berlin, 2010)
10. Q. Luo, W. Liu, S.L. Chin, Appl. Phys. B **76**, 337 (2003)
11. J.P. Yao, B. Zeng, H.L. Xu, G. Li, W. Chu, J. Ni, H. Zhang, S.L. Chin, Y. Cheng, Z.Z. Xu, Phys. Rev. A **84**, 051802 (2011)
12. H.L. Xu, E. Lötstedt, A. Iwasaki, K. Yamanouchi, Nat. Commun. **6**, 8347 (2015)
13. V. Andreeva, O. Kosareva, N. Panov, D. Shipilo, P. Solyankin, M. Esaulkov, P. Martínez, A. Shkurinov, V. Makarov, L. Bergé, S.L. Chin, Phys. Rev. Lett. **116**, 063902 (2016)
14. N. Akozbek, A. Iwasaki, A. Becker, M. Scalora, S.L. Chin, C.M. Bowden, Phys. Rev. Lett. **89**, 143901 (2002)
15. T. Popmintchev, M.C. Chen, D. Popmintchev, P. Arpin, S. Brown, S. Alisauskas, G. Andriukaitis, T. Balciunas, O.D. Mucke, A. Pugzlys, A. Baltuska, B. Shim, S.E. Schrauth, G. Gaeta, C. Hernandez-Garcia, L. Plaja, A. Becker, A. Jaron-Becker, M.M. Murnane, H.C. Kapteyn, Science **336**, 1287 (2012)
16. H.L. Xu, Y. Kamali, C. Marceau, P.T. Simard, W. Liu, J. Bernhardt, G. Mejean, P. Mathieu, G. Roy, J.-R. Simard, S.L. Chin, Appl. Phys. Lett. **90**, 101106 (2007)
17. H.L. Xu, G. Méjean, W. Liu, Y. Kamali, J.-F. Daigle, A. Azarm, P.T. Simard, P. Mathieu, G. Roy, J.-R. Simard, S.L. Chin, App. Phys. B **87**, 151 (2007)
18. H.L. Xu, P.T. Simard, Y. Kamali, J.-F. Daigle, C. Marceau, J. Bernhardt, J. Dubois, M. Châteauneuf, F. Théberge, G. Roy, S.L. Chin, Laser Phys. **22**, 1767 (2012)
19. H.L. Xu, S.L. Chin, Sensors **11**, 32–53 (2011)
20. H.L. Xu, Y. Cheng, S.L. Chin, H.B. Sun, Laser Photonics Rev. **9**, 275 (2015)
21. H.L. Li, W. Chu, H. Zang, H.L. Xu, Y. Cheng, S.L. Chin, Opt. Expr. **24**, 3424 (2016)
22. V.I. Talanov, Sov. Phys. JETP Lett. **11**, 199 (1970); J.H. Marburger, Prog. Quantum Electron. **4**, 35 (1975)
23. W. Liu, S.L. Chin, Opt. Expr. **13**, 5750 (2005)

24. V. Loriot, E. Hertz, O. Faucher, B. Lavorel, Opt. Expr. **18**, 3011 (2010)
25. S.L. Chin, A. Talebpour, J. Yang, S. Petit, V.P. Kandidov, O.G. Kosareva, M.P. Tamarov, Appl. Phys. B **74**, 67 (2002)
26. H.L. Li, X.Y. Wei, H.L. Xu, S.L. Chin, K. Yamanouchi, H.B. Sun, Sens. Actuators B Chem. **203**, 887 (2014)
27. R.W.B. Pearse, A.G. Gaydon, in *The Identification of Molecular Spectra*, 4th edn. (Chapman & Hall, UK, 1976)
28. J. Chen, R. Ma, H. Ren, X. Li, H. Yang, Q. Gong, Int. J. Mass Spectrom. **241**, 25 (2005)
29. H. Li, H. Xu, B. Yang, Q. Chen, T. Zhang, H. Sun, Opt. Lett. **38**, 1250 (2013)
30. H. Li, W. Chu, H.L. Xu, Y. Cheng, S.L. Chin, K. Yamanouchi, H.B. Sun, Sci. Rep. **6**, 27340 (2016)
31. H.W. Zang, H.L. Li, Y. Su, Y. Fu, M.Y. Hou, A. Baltuška, K. Yamanouchi, H.L. Xu, Opt. Lett. **43**, 615 (2018)
32. P. Minutolo, G. Gambi, A. D'Alessio, S. Carlucci, Atmos. Environ. **33**, 2725 (1999)